

Roughness-Induced Instability in a Laminar Boundary Layer at Mach 6

Bradley M. Wheaton* and Steven P. Schneider†

School of Aeronautics and Astronautics, Purdue University, West Lafayette, IN 47907-1282

Roughness can cause a boundary layer to become turbulent, increasing aeroheating from the laminar rate. Empirical correlations are currently extrapolated to predict the onset of roughness-induced transition but are only simple approximations of the flow physics that cause it. More accurate physics-based prediction methods must be developed, based on the growth of instabilities within the wake of the roughness. A cylindrical roughness element was used to introduce instabilities into a laminar nozzle-wall boundary layer in the Boeing/AFOSR Mach-6 Quiet Tunnel. Pitot and hot-wire probes were used to measure an instability in the wake of the roughness. These measurements are believed to be the first at hypersonic speeds. The instability was observed to grow downstream of the roughness and was strongest off the wake centerline at a height near the roughness height. Mean-flow pitot pressures in the wake of the roughness were recorded for comparison to future computations of the wake. Further characterization of this instability can assist development and validation of a physics-based prediction method for roughness-induced transition.

Nomenclature

δ	boundary-layer thickness, defined as the height where the local velocity is 99.5% of the freestream value	u	velocity (m/s)
ρ	density (kg/m ³)	y	probe height above wall (mm)
D	cylindrical roughness diameter (mm)	z	tunnel axial coordinate (0 at throat) (in)
k	cylindrical roughness height (mm)	<i>Subscript</i>	
M	Mach number	∞	freestream condition
p	pressure (psia or kPa)	0	tunnel stagnation condition
Re_k	Reynolds number based on roughness height k and local conditions in the undisturbed laminar boundary layer at the height k	i	initial condition
Re_∞	freestream unit Reynolds number (/ft)	<i>Abbreviations</i>	
t	tunnel run time (s)	BAM6QT	Boeing/AFOSR Mach-6 Quiet Tunnel
T	temperature (K)	LST	Linear Stability Theory
		PLIF	Planar Laser-Induced Fluorescence
		PSE	Parabolized Stability Equations
		RMS	Root Mean Square

I. Introduction

A. Hypersonic Boundary-Layer Transition

Accurate prediction of boundary-layer transition is desired to predict heating and skin friction on a hypersonic flight vehicle. Boundary-layer transition is caused by the growth of disturbances which originate in the freestream or on the body, and interact with instabilities in the boundary layer.¹ The transition location is influenced by many factors and thus is difficult to simulate and predict. These factors include freestream Reynolds number, Mach number, wall temperature, mass addition, freestream disturbances, and surface

*Research Assistant, Student Member AIAA

†Professor, Associate Fellow AIAA

roughness.² In addition, many different physical mechanisms within the boundary layer can cause transition,³ but these mechanisms are poorly understood. Because of the complexities involved in the transition process, empirical correlations are often used to predict the location of transition for hypersonic flight vehicles.

B. Effect of Roughness on Hypersonic Transition

Among the many factors that can influence hypersonic transition is surface roughness. Roughness on the surface of a reentry vehicle can cause early transition and higher heating in flight.⁴ This roughness can be classified as either: (1) distributed, such as sandpaper-type roughness, an ablating heat shield, or machining patterns, or (2) isolated. Examples of isolated (also called discrete) roughness elements include protrusions such as space shuttle gap fillers or capsule tie rods, steps, gaps, and surface flaws or imperfections. Isolated roughness elements can also be used to intentionally trip an existing laminar boundary layer, for instance to prevent scramjet engines from unstating.^{5,6} Research is needed to determine if a naturally-occurring roughness will cause transition during reentry, or to determine the largest roughness that will begin to affect the natural transition location.

A discrete roughness element (if it is large enough) generally causes transition to occur earlier than it would in the smooth-wall case, with the transition location moving closer to the roughness as the height of the roughness is increased. A roughness can be small enough to have no effect on the transition location, in which case the roughness height is below its critical height. At heights larger than the critical height, the transition location moves closer to the roughness element. As the roughness height is increased further, the transition location will move to its closest location behind the roughness. This height is the effective height, beyond which the transition location does not move. Both the critical and effective roughness heights can be influenced by factors such as roughness shape or freestream noise conditions.⁷

The roughness-induced transition process is poorly understood, and this fact was highlighted in July 2005 during Space Shuttle Mission STS-114. During the mission, a gap filler became dislodged and protruded from the thermal protection system (Figure 1(a)). It was unknown exactly how this gap filler would affect transition during re-entry. Due to this uncertainty, the gap filler was removed in orbit by an astronaut, prior to re-entry (Figure 1(b)). If roughness-induced transition was better understood, perhaps this spacewalk could have been avoided. Recent high-profile flight experiments on the Space Shuttle are visible examples of the effort to understand roughness-induced transition.^{8,9}

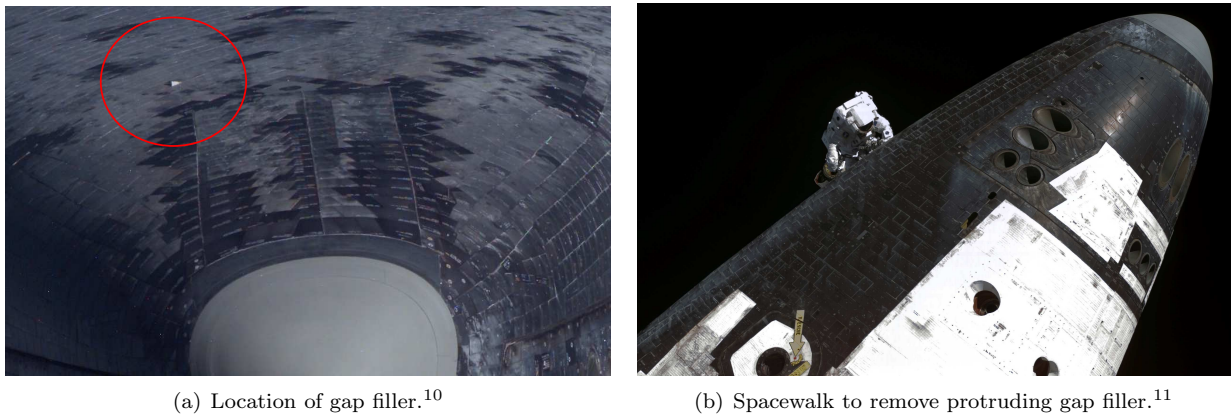


Figure 1. Example of an isolated roughness: protruding gap filler on Space Shuttle Mission STS-114, removed by astronaut in orbit

1. Current Prediction Methods

Much previous research was concerned only with transition locations and flow conditions, to collect data for engineering correlations.⁴ Correlations are used with some success for many flight vehicles and are based on parameters such as Re_k , the Reynolds number at the roughness height k based on conditions in the undisturbed laminar boundary layer at the height k .¹² Correlations, however, are only simple approximations of the flow physics behind the roughness and are often extrapolated. If correlations are not used carefully they can lead to large uncertainties in transition location. Measurements made for correlations in ground facilities

may be subject to noise effects, which can significantly alter the roughness-induced transition location.⁷ It is both difficult and expensive to gather flight transition data for correlations. In the future, prediction methods that are based on the computed growth of instabilities in the wake of a roughness element are desired to reduce uncertainty in predicting roughness-induced transition.

2. Mechanisms By Which Roughness Affects Transition

To develop computational models for predicting roughness-induced transition, the physical mechanisms leading to transition must be characterized. Though significant progress has been made in understanding these mechanisms, they are not fully understood. There appear to be at least four ways that roughness can cause transition:

1. instabilities within the roughness wake causing transition
2. the steady wake of the roughness interacting with other instability mechanisms to cause transition
3. freestream disturbances interacting with roughness via a receptivity process to generate instabilities
4. roughness modifying the amplification of existing instabilities in the smooth-wall boundary layer

There is no general theory for determining which mode will dominate the transition process. The dominant mode may depend on roughness type (isolated or distributed), roughness geometry and spacing, freestream flow conditions, and any number of other factors. The first category, where instabilities induced by the roughness wake cause transition, is the most understood of the three. It is also the most likely cause for transition behind a large isolated roughness element, and thus will be explained in more detail here.

A roughness element may often generate a wake with large streamwise vorticity. These streamwise vortices could be steady distortions of the mean flow or they could break down and cause transition. Oil-flow visualization by Whitehead¹³ showed several large streamwise vortices within the wake of roughness elements on a rectangular wedge model in Mach 6.8 flow. Figure 2, a photograph from Whitehead's report, shows oil flow patterns around tripping elements of various shapes. The local edge Mach number was 5.5 and the roughness height k was twice the boundary-layer thickness δ . The vortices are seen wrapping around the roughness and are oriented in the streamwise direction farther downstream. The vortices were observed to persist even into the turbulent portion of the wake.

Recent flow visualization by Danehy et al.¹⁴ showed streamwise vortices within the wake of a roughness element, breaking down into turbulence as they convected downstream. Nitric oxide planar laser-induced fluorescence (PLIF) was used to visualize the flow in a plane parallel to the surface behind a 2-mm-radius hemispherical roughness. Figure 3 shows two images from these tests, which were conducted in the NASA Langley 31-in. Mach 10 Tunnel. The two images were taken at freestream unit Reynolds numbers of $3.3 \times 10^6/\text{m}$ and $6.1 \times 10^6/\text{m}$, respectively. In the images, flow is from left to right and the height of the laser sheet was not explicitly specified. A shadow is produced on one side of the roughness, caused by the blockage of the laser sheet. The vortex pattern can be seen in both images and the vortices appear more unstable in the higher Reynolds number test.

The dominant mechanism for transition could be an absolute instability such as periodic vortex shedding, similar to that observed at low speeds by Acarlar and Smith.¹⁵ Their experiments showed periodic shedding of "hairpin" vortices in the wake of a hemispherical roughness. The role of absolute instabilities in roughness-induced transition at high speeds is not well known. Figure 4 shows computational results for vortex shedding behind a 2D roughness at subsonic edge conditions.¹⁶ The vortex shedding was not observed at supersonic edge conditions, though it remains unclear why.

In addition to large vortical disturbances, a roughness generates shear layers which can foster the growth of convective instabilities. These instabilities grow in the shear layer as they convect downstream from the roughness and may be the dominant mechanism for transition behind an isolated roughness at high speeds.¹⁶ The compressibility of high-Mach-number flow tends to have a stabilizing effect on the mean flow,¹⁷ suggesting that the transition process could be thought of as "a race between unsteady fluctuation growth (in the unstable wake) and the rapid relaxation of the basic state toward a spanwise-uniform Blasius flow".¹⁸ The convective instabilities in the shear layers generated by the roughness may exist even in the absence of large vortical disturbances.¹⁶ The modal shape and growth rates of shear-layer instabilities in a hypersonic roughness wake have recently been computed by Choudhari et al.¹⁷

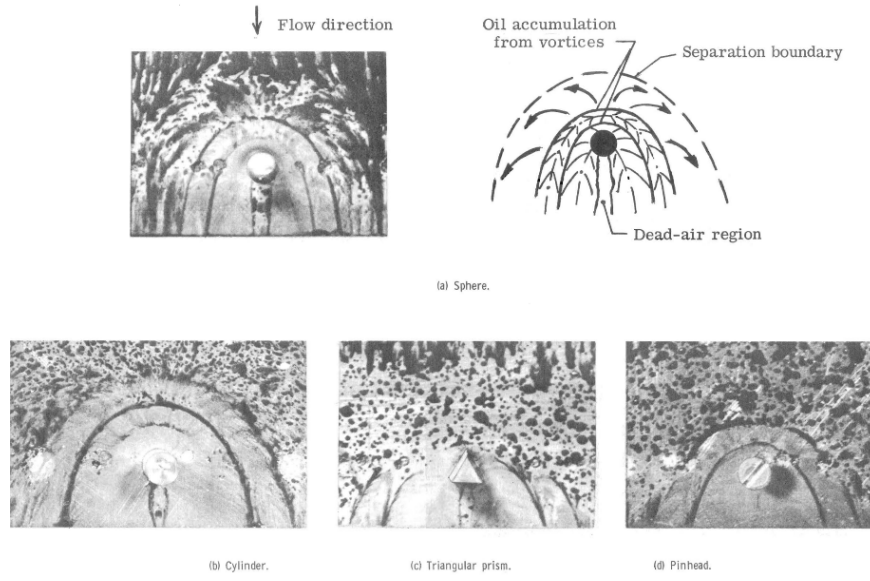


Figure 2. Oil-flow patterns of roughness elements, showing presence of streamwise vortices as well as separation regions (images from Reference 13). The local edge Mach number was 5.5 and $k/\delta = 2$.

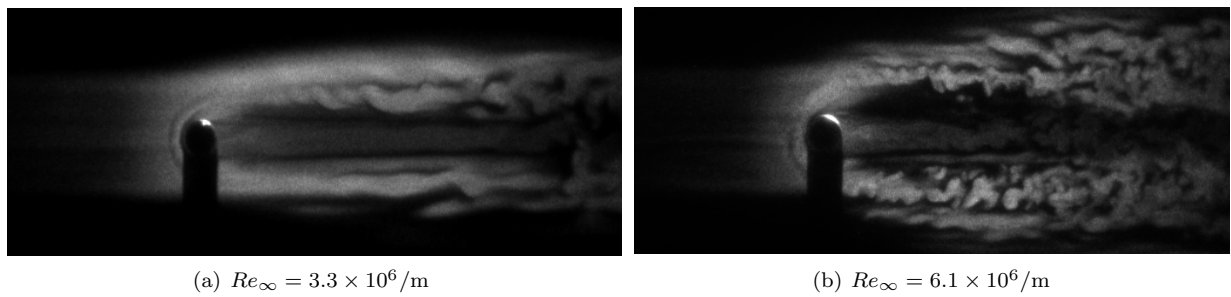


Figure 3. Streamwise vortices in the wake of a 2-mm-radius hemispherical roughness using nitric oxide planar laser-induced fluorescence (PLIF). Plan view with flow from left to right. Images from Figures 11 and 12 in Reference 14.

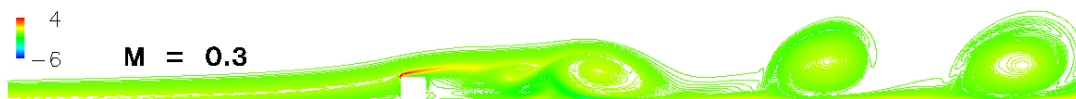


Figure 4. Side view of vortex shedding behind a 2D roughness at low speed. Flow is from left to right and vorticity contours are shown. Image from Figure 12(a) in Reference 16.

The remaining three categories from above are also possible paths to roughness-induced transition. Instead of transition being caused by instabilities in the roughness wake, the steady wake with streamwise vorticity could also interact with existing instabilities within the boundary layer to cause transition. Reshotko and Tumin¹⁹ explore transient growth as a mechanism for both discrete and distributed roughness. These streamwise vortices could also grow via an interaction with the Görtler instability or stationary crossflow.⁴ Roughness could act as a modifier to receptivity in a boundary layer, most likely for distributed roughness that is either random or periodic in nature.²⁰ Roughness can also modify the amplification of the instabilities that exist in the smooth-wall boundary layer, but this effect is probably not significant.

C. Measuring Roughness-Wake Instabilities in the Boeing/AFOSR Mach-6 Quiet Tunnel

Ideally, the growth of roughness-induced instabilities would be used to predict the location of transition (e.g. Klebanoff²¹). A semi-empirical transition prediction method such as the e^N method can be used to reduce uncertainty in the roughness-induced transition location for hypersonic vehicles. However, these computational methods must be developed and validated with experimental measurements.

Future computations will require detailed measurements of the growth of instabilities within the roughness wake. Ergin and White reported detailed hot-wire measurements of instabilities in the wake of cylindrical roughness elements at low speed.¹⁸ At high speed, however, it is difficult to make detailed wake measurements. A laminar boundary layer for testing roughness elements is desired, but boundary-layer heights on models in hypersonic test facilities are often small (on the order of 1 mm or less). A thicker boundary layer is desired for three reasons:

1. A thick boundary layer would increase the spatial resolution of instability measurements
2. A thick boundary layer can be used to reduced the effects of probe interference with the flow, so larger probes could be used
3. The frequencies of instabilities would theoretically be reduced in a thicker boundary layer

The nozzle wall of the Boeing/AFOSR Mach-6 Quiet Tunnel (BAM6QT) at Purdue University was used to provide the thicker boundary layer desired for these experiments. The BAM6QT can be operated with a laminar boundary layer up to 20 mm thick, an order of magnitude larger than a typical model boundary layer. A variable-height cylindrical roughness element was therefore used to introduce instabilities into the nozzle-wall boundary layer. There, detailed measurements of instabilities can be made in support of future computations. Together with the computations, the instability measurements will help support development of semi-empirical physics-based transition prediction for isolated roughness elements in hypersonic flow.

II. Experimental Approach

A. Boeing/AFOSR Mach-6 Quiet Tunnel

The Boeing/AFOSR Mach-6 Quiet Tunnel (BAM6QT) at Purdue University is a low-noise hypersonic facility used mainly for transition research.²² The tunnel has recently been the only operational hypersonic quiet tunnel in the world and has noise levels less than 0.05% during quiet-flow operation.²³ The BAM6QT is a blowdown facility using a Ludwig tube design, consisting of a long tube with a converging-diverging nozzle (Figure 5). During operation, the upstream portion of the tunnel is filled with high-pressure air while the region downstream of the diffuser is evacuated. Diaphragms are then broken to initiate the flow. During the typical 3–5 s run time, the pressure in the driver tube drops quasi-statically and the freestream Reynolds number decreases. The maximum stagnation pressure for quiet flow operation is currently above 160 psia.²⁴

A laminar boundary layer on the nozzle wall of the BAM6QT enables low-noise operation, but was also desired for for making measurements of instabilities induced by a roughness element. Several design features permit the tunnel to be operated with a laminar boundary layer on the nozzle wall.²³ Upstream of the throat, a bleed slot is used to remove the existing boundary layer. A new laminar boundary layer then begins at the throat. The interior of the nozzle is polished to a mirror finish to reduce roughness that could trip the laminar boundary layer. Great care is taken to ensure that dust or other small particles do not infiltrate this section of the nozzle, as even a small particle could decrease quiet flow performance. To reduce instabilities, the nozzle has a circular cross section and is longer than a conventional nozzle to decrease concavity. A more detailed discussion of the components of the BAM6QT appears in Reference 25.

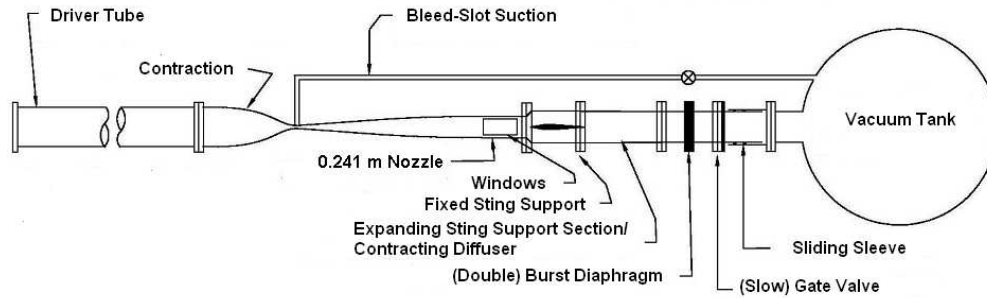


Figure 5. Schematic of the Boeing/AFOSR Mach-6 Quiet Tunnel.

B. Roughness Element

A Starrett model 263L-38TN micrometer head was used as a cylindrical roughness element (Figure 6(a)). The height k of the 5.97-mm-(0.235-in.-)diameter roughness element can be changed from 0.00–24.31 mm and is accurate to ± 0.05 mm. The roughness element was located in the nozzle of the BAM6QT at tunnel coordinate $z = 1.924$ m (75.749 in.), mounted in a specially-designed circular insert in an upstream window insert (Figure 6(b)). Since the four upstream window sections of the BAM6QT nozzle are interchangeable, the roughness element can be placed on either the lower wall or side wall. The lower-wall configuration was used for hot-wire and pitot-probe measurements while the side-wall configuration was used for temperature-sensitive paint measurements as in Reference 7. Three locations in the circular insert allow the spanwise position of the roughness element to be changed, so that measurements can be taken off the center of the wake. The circular insert has a location in the center as well as ± 2.0 diameters off-center. More inserts are currently being manufactured to allow measurements in different spanwise planes of the roughness wake. The new inserts will allow measurements to be made at 0.5, 1.0, and 1.5 diameters off the roughness centerline.



(a) Close-up view.



(b) View of roughness installed in nozzle insert.

Figure 6. Variable-height cylindrical roughness element with 0.235-in. diameter.

C. Apparatus for Instability Measurements

Pitot and hot-wire probes were used in the wake of the roughness element to search for evidence of flow instabilities. A common apparatus was used for both probe types, because the pitot probe and hot-wire probes were similarly shaped. A large angled probe support was used to hold the probes and make measurements upstream in the nozzle, near the roughness element location. Figure 7 shows an example of the setup used for pitot-pressure measurements. The image was taken looking upstream through the nozzle. The left hand side of the image shows the nozzle wall hot-film array. The signals from two wall hot films are monitored during each run to ensure that the nozzle-wall boundary layer is laminar and attached. Because the hot-film

array was offset 90° from the roughness, the wake of the roughness was not expected to interfere with the boundary layer there. The right hand side of the image shows the large plexiglass window. The roughness element is visible on the lower wall of the tunnel. Downstream of the roughness, the pitot probe and angled probe support can be seen. The probe support was installed on the tunnel centerline using the traverse system and suspended through a slot on the top wall of the tunnel. The pitot probe was installed in the angled probe support and the probe wires were protected from the flow using high-temperature tape. The probe was then placed at various streamwise positions prior to each run.

Measurements were taken with the probe stationary as well as traversing vertically during a run (perpendicular to the tunnel centerline). As a result of the decreasing stagnation pressure, measurements taken during a single run contain variations in Reynolds number. For a quiet-flow run at $p_{0,i} = 90$ psia, the Reynolds number decreases by approximately 10–15% in 3 s. This variation offers an advantage because frequency-shifting of instabilities can be observed as the freestream Reynolds number changes. However, an accurate profile of the nozzle-wall boundary layer at a given Reynolds number cannot be measured during a single run.

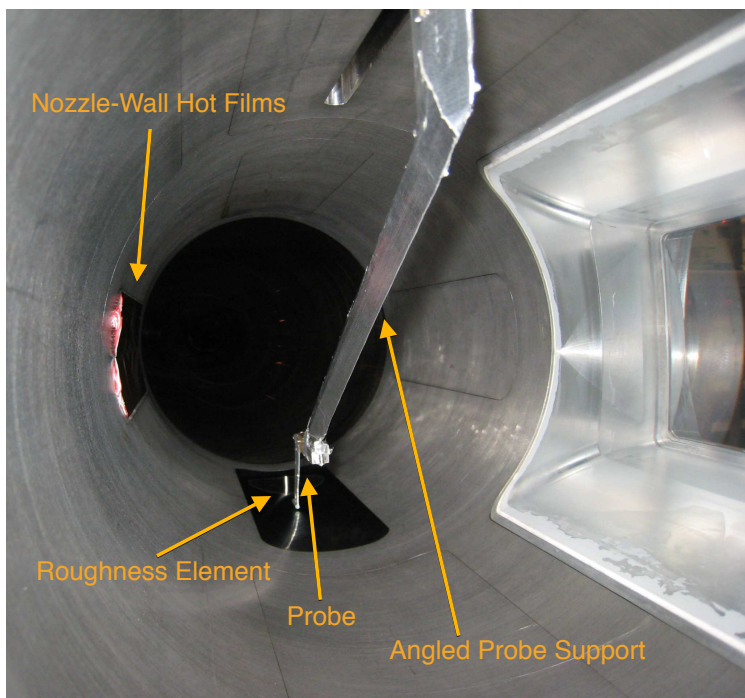


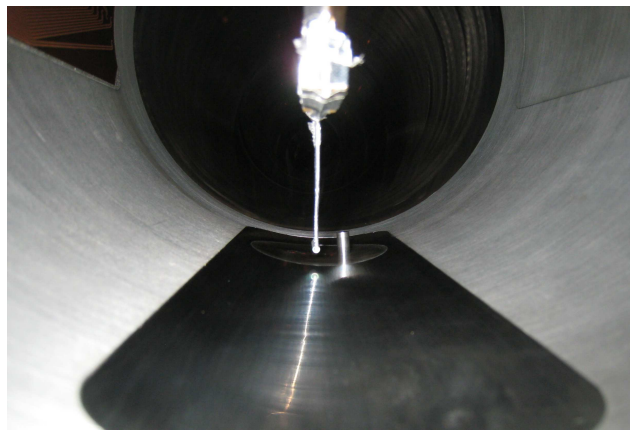
Figure 7. Configuration for pitot-probe measurements, looking upstream through the nozzle. A similar configuration was used for hot-wire measurements.

The roughness height k was adjusted prior to each run and the probe always remained on the tunnel centerline. The roughness was moved between three spanwise locations to make measurements both on and off the centerline of the wake. Figure 8(a) shows a close-up view of the roughness insert, with the roughness positioned two diameters off-center from the probe (11.94 mm or 0.47 in.). In the image, flow is from left to right and the pitot probe is located approximately 7.6 mm (0.3 in.) downstream of the roughness. In this configuration, the measurements are taken in a plane two diameters off-center from the roughness. The roughness was also placed in the center position to make measurements on the centerline behind the roughness. Figure 8(b) shows the off-centerline measurement configuration from behind the probe, looking upstream. Due to curvature in the tunnel wall, the plane of the off-center measurements is not parallel to the roughness element. The plane is angled 5.7° with respect to the roughness element. This effect would have to be considered when comparing results to precise numerical computations.

Possible problems with the apparatus were explored in detail in Reference 25. Both probe vibration and shock-induced boundary-layer separation could cause oscillations in the probe signals that could be mistaken for instabilities. A test-bench experiment was performed using the long probe support to determine its natural vibrational frequencies. The test results along with observations in the BAM6QT led to a belief that the



(a) Flow is from left to right. A scale with tenths and hundredths of inches is shown.



(b) View of pitot probe and roughness, looking upstream.

Figure 8. Example of measuring two diameters off of the roughness centerline.

vibration of the probe support occurs at low frequencies, on the order of 20 Hz. This frequency is orders of magnitude lower than expected frequencies of instabilities and thus should not interfere with measurements.

Several methods were used to control separation of the nozzle-wall boundary layer caused by the diffuser section and its various inserts.²⁶ This separation was visible as a large low-frequency oscillation that occurred simultaneously on the signals from the probe and wall hot films. In the case of nozzle-wall boundary-layer separation, all data were discarded except for some mean-flow data appearing in Figure 10. The largest concern for the apparatus remains the possibility of a complicated shock/boundary-layer interaction between the probe, probe support, and roughness.

D. Probe Types

Two probe types were used within the wake of the roughness element to measure instabilities: (1) calibrated and uncalibrated hot-wire probes and (2) a pitot probe with a Kulite piezoelectric pressure transducer. Both probes had similar geometry and mounts, so that they could be used interchangeably within a similar apparatus (Figure 9). The probes feature a 51-mm-(2-in.-)long knife-edged strut to probe the thick nozzle-wall boundary layer with minimal flow interference.



(a) Hot-wire probe (typical)



(b) Pitot probe with unmounted sensor

Figure 9. Photographs of the two types of probes used for instability measurements. Each probe had a 2-in.-long strut to probe the thick nozzle-wall boundary layer with minimal flow interference.

1. Uncalibrated and Calibrated Hot Wires

The four hot-wire probes used to measure instabilities were built at Purdue University specifically for operation in the thick nozzle-wall boundary layer, as shown in Figure 9(a). Earlier hot-wire probes^{27, 28} used in the BAM6QT had shorter struts that would have increased interference on the nozzle wall. The probes have stainless-steel bodies and used 0.0002-in.-diameter Platinum–10% Rhodium wires for these experiments. A TSI IFA-100 constant-temperature anemometer with a 1:1 bridge was used to control the wire temperature and provide an output voltage. A control resistor was used to “set” the wire temperature, and the resistance ratio between the control resistor and probe resistance was chosen to be 1.7–1.9, as recommended by Rufer.²⁸ To record data, the output voltage of the anemometer was connected via a BNC cable to an oscilloscope.

Both uncalibrated and calibrated results from hot-wires are reported. In the case of the calibrated results, a mass-flux calibration was performed in the freestream of the BAM6QT with no roughness present. Three runs at various initial stagnation pressures were performed and the anemometer voltage was recorded. The mass flux was calculated during each run using the stagnation pressure, assumed freestream Mach number, the perfect gas law, and an isentropic assumption for the decreasing stagnation temperature during the run.

The hot-wire probes offered several advantages over the Kulite pitot probe (Table 1). Because the wire diameters are so thin, hot wires are capable of a high frequency response (up to 200-300 kHz depending on the wire diameter used). In addition, the wire is thought to have low flow interference. A 0.0002-in.-diameter wire is approximately 0.05% of the nozzle-wall boundary-layer thickness at the tunnel conditions where most instability measurements were made, though the 1/32-in.-thick strut holding the wire has more blockage. However, the hot wires are fragile and often break, especially during tunnel startup and shutdown. The hot wires are also sensitive to electronic noise from the stepper-motor that drives the traverse system. Thus, the traverse system was not used during hot-wire measurements and the hot wires were left at a constant position during the runs.

2. Kulite Pitot Probe

A Kulite XCQ-062-15A piezoelectric pressure transducer was used in a pitot probe to make dynamic measurements of disturbances in the thick nozzle-wall boundary layer. The sensor had a diameter of 1.68 mm (0.066 in.) and a range of approximately 0–15 psia. A mechanical stop at pressures greater than 15 psia protects the sensor from damage as the tunnel is filled to stagnation pressure prior to a run. Custom electronics are used to power and process the voltage output of the transducer. The Kulite was calibrated while installed in the tunnel, using the vacuum that exists after a run ends.

A new probe was designed to hold the sensor, with a design similar to the hot-wire probes (Figure 9(b)). The probe consists of a body section with a 51-mm-(2-in.-)long knife-edged strut to hold the Kulite sensor. The 1.68-mm-diameter sensor is mounted in a 3.18-mm-(0.125-in.-)diameter tube at the base of the strut. The upstream end of the tube was tapered to decrease interference. The Kulite was held in place using nail polish and the wire was taped to the back of the strut using high-temperature tape.

Though hot wire probes are the preferred instrument for making measurements of instability waves in a boundary layer, the use of a Kulite pitot probe offered several advantages (Table 1). Primarily, a Kulite is robust and not susceptible to breakage like a hot wire. A Kulite is also less sensitive to electronic noise than a hot wire, allowing the stepper-motor that drives the traverse system to be used without interference in the output signal.

The Kulite cannot achieve as high a frequency response as a properly tuned hot wire. The frequency response of the pitot-probe sensor was estimated to be 60–70 kHz, based on 20% of the observed resonance frequency. However, the frequencies of instabilities within the thicker nozzle-wall boundary layer should be smaller than those typically measured in boundary layers on models, and the lower frequency response of the Kulite may be sufficient. The pitot probe also has more flow interference than a hot-wire probe, but the exact effect of flow interference is difficult to quantify. The diameter of the Kulite sensor is approximately 20% of the boundary-layer thickness on the nozzle wall at the tunnel conditions where instability measurements were made. Finally, the Kulite sensor is subject to resonance of the sensor diaphragm. This resonance always occurred at 330 kHz, and sometimes had a large amplitude (particularly in regions of higher turbulence). Since the resonance frequency was an order of magnitude larger than the frequencies of interest (less than 50 kHz), it was assumed that the resonance did not affect these frequencies. The data were sampled at high frequencies to avoid any aliasing which might occur due to the resonance (see Section E).

Table 1. Advantages and disadvantages of each probe type.

Hot-Wire Probes	Kulite Pitot Probe
Higher frequency response (+)	Lower frequency response (-)
Low flow interference (+)	More flow interference (-)
Low survival rate (-)	Robust (+)
Sensitive to traverse electronic noise (-)	Insensitive to traverse noise (+)
	Sensor resonance at 330 kHz (-)

E. Data Acquisition and Analysis

1. Acquisition

Probe data were sampled at 2.0 MHz in Hi-Res mode on a Tektronix DPO7054 Oscilloscope. Hi-Res mode is a method of digital filtering in which the scope samples at its maximum sampling frequency of 500 MHz and digitally averages on the fly to the desired sampling frequency of 2.0 MHz (averaging 250 points per data point). This mode effectively acts as a low-pass filter to eliminate signal aliasing. In addition, Hi-Res mode decreases noise and increases the number of vertical bits of resolution (from 8 to approximately 12–13).

2. Post-Processing and Analysis

MATLAB was used for all post-processing of data. The probe data were separated into 0.05-s samples of 100,000 points each. The 0.05-s sample time was the time during which the probe was stationary when using the traverse system. Mean pitot pressures and hot-wire mass fluxes were calculated from the mean of the 100,000-point samples.

All spectra were plotted as root-mean-square spectra to provide a quantitative amplitude on the vertical axis. Each spectrum was computed from the 0.05-s sample. Blackman windows with 5,000 points and 50% overlap were used, resulting in a total of 30 windows from the 100,000-point sample. The spectral amplitudes represent the RMS of the signal over the frequency bands, and thus the amplitudes vary depending on the frequency spacing. All spectra were computed to achieve a frequency spacing of 0.24 kHz. Because the mean pitot pressure was changing at each point, the spectra were normalized by the theoretical freestream pitot pressure. This value was the stagnation pressure behind a normal shock at Mach 6, or 2.965% of the freestream stagnation pressure. A pre-run Kulite spectra was not available due to the settings in the vertical resolution of the oscilloscope. A separate pre-run trace was not obtained. Uncalibrated hot-wire spectra were reported as raw voltage fluctuations while calibrated hot-wire spectra were nondimensionalized by the measured mean mass flux.

A more representative RMS was obtained by integrating the area under the power spectrum of the signal. The power spectral density was computed from the 100,000-point sample using Welch’s method and achieving a frequency spacing of 0.24 kHz. The units of amplitude for the power spectra were psia^2/Hz or $(\text{kg}/\text{s}\cdot\text{m}^2)^2/\text{Hz}$. The RMS of frequency bands of interest was calculated by numerically integrating the area under the power spectrum. The integration resulted in the power of the frequency band in psia^2 or $(\text{kg}/\text{s}\cdot\text{m}^2)^2$. The square root of that number gave the RMS of the frequency band.

III. Boundary-Layer Mean-Flow Measurements

Mean-flow measurements in the nozzle-wall boundary layer were taken for comparison to computational solutions, both with and without the roughness element. The Kulite pitot probe was mounted on the angled probe support and was used to make measurements in the wake of the roughness element. All mean-flow results were collected under quiet flow conditions. The 0.24-m-diameter pipe insert²⁶ (without the pipe insert extension²⁴) was installed in the sting-support section with no gap present. Both the mean pitot pressure and the pressure fluctuations were recorded for various freestream Reynolds numbers, roughness heights, and locations within the wake. All mean pitot pressures were nondimensionalized by the freestream stagnation pressure. Smooth-wall measurements will be reported here, along with measurements in the wake

of a 10.2-mm roughness. Additional results can be found in Reference 25.

A. Smooth-Wall Measurements

Measurements of the nozzle-wall boundary layer in the absence of the roughness element were performed at an initial stagnation pressure ($p_{0,i}$) of 90 psia. The stagnation pressure was chosen because it was high enough to avoid major problems with separation of the nozzle-wall boundary layer, and low enough to increase hot-wire survival, should hot-wires be used at similar conditions.

In order to measure a wider range of heights above the wall, several runs must be performed. The probe measurement range is limited by several factors, mainly the run time of the BAM6QT. The time at each data point, distance between points, and traverse acceleration and velocity can be adjusted as desired to maximize the number of data points measured before the end of the run. Figure 10 shows mean pressure data from four smooth-wall runs at an initial stagnation pressure of 90 psia, measuring at $z = 78.6$ in. (2.00 m). For each run, the initial height above the wall y_i was varied as well as the movement direction of the probe. The distance between points was 0.635 mm for all four runs. Computations at a similar streamwise location were obtained using the Harris code.²⁹ The pressures from different runs show relatively good agreement, except near the wall. The disagreement near the wall may result from some boundary-layer separation that was present near the end of the run when moving towards the wall. The boundary-layer separation created oscillations which could have affected the calculation of mean pressure.

The boundary-layer height was roughly 9–10 mm and the mean pitot pressure approached the theoretical freestream value away from the wall. The pitot pressure “overshoots” the theoretical value near the boundary-layer edge. This overshoot is possibly a result of probe interference caused by the relatively large sensor diameter, as in References 30 and 31. However, the overshoot is not large and the majority of the pitot-pressure data appear to agree well. The freestream pitot pressure indicates a Mach number near 5.95, which is confirmed by the computations. In the BAM6QT, the freestream Mach number is only 6.0 near the nozzle exit at $z = 101.975$ in, for a stagnation pressure of 150 psia. Upstream of the nozzle exit and near the wall, the freestream Mach number will be slightly less than 6.0 due to the expanding nozzle area. Lower stagnation pressures will have a similar effect because the boundary layer will be thicker.

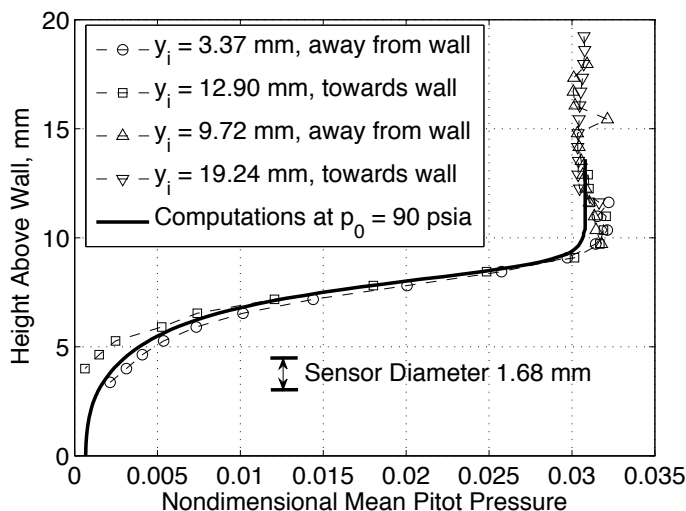


Figure 10. Smooth-wall boundary layer at $z = 78.6$ in. (2.00 m) when $p_{0,i} = 90$ psia. Data from four runs with various initial heights above the wall and movement directions. Pitot pressure nondimensionalized by freestream stagnation pressure.

B. Mean-Flow Pitot Pressures in a 10.2-mm Roughness Wake

Mean pitot pressures were recorded at a number of locations downstream of a $k = 10.2$ mm roughness element during measurements of the flow instability. The pitot probe was positioned two diameters off-center from the roughness element and runs were performed with an initial stagnation pressure of 90 psia. Measurements

were taken during multiple runs at 2, 3, 5, and 10 diameters (D) downstream of the roughness. At each streamwise position, 2–3 runs were performed with different initial heights above the wall and different movement directions. Data were acquired at vertical intervals that varied between 0.3, 1.0, and 2.0 mm.

The results are plotted in Figure 11. During each run, the Reynolds number changed by roughly 10%, and differences in pitot pressures between two similar heights can be attributed to Reynolds number differences. Smooth-wall data at $z = 76.1$ in., near the location where the roughness is placed, are also plotted for comparison. The measurements in the wake of the roughness show an overshoot of the theoretical Mach-6 value of 0.2965, followed by a sudden decrease in pressure. This trend is more visible at 5 and 10 roughness diameters downstream where the pitot pressure decreases by 30–40% within a few millimeters. The rapid decrease in pressure was assumed to indicate the location of a shock; it corresponded to a peak in the RMS pressure. The assumed shock locations are denoted by boxes in Figure 11 and are summarized in Table 2. A plot of the assumed shock locations versus streamwise distance appears in Figure 12 and a linear fit to the four points shows the shock shape. The linear fit does not originate from the top of the roughness element, however; the measurements were taken in a plane two diameters off-center from the roughness. Computations are needed to determine if an actual shock location has been found.

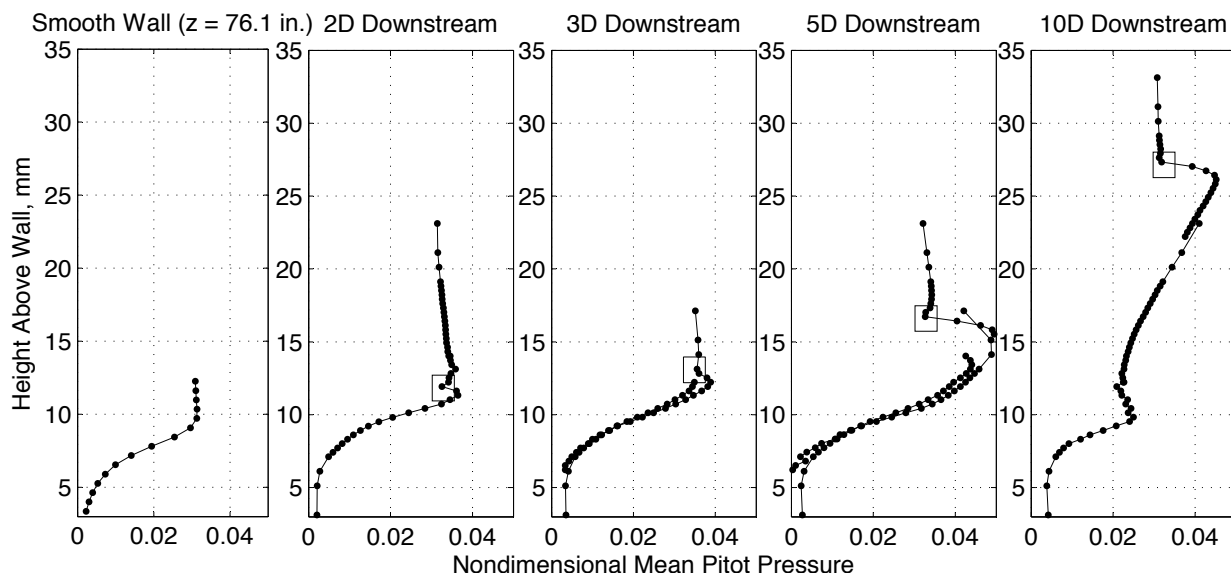


Figure 11. Mean pitot pressures at several streamwise distances behind the 10.2-mm roughness and two diameters off the centerline. Pitot pressure nondimensionalized by freestream stagnation pressure. Boxes denote assumed shock location. Multiple runs at $p_{0,i} = 90$ psia. Conditions typically varied from $p_0 = 87$ psia, $T_0 = 430$ K, and $Re_\infty = 2.00 \times 10^6/\text{ft}$ to $p_0 = 70$ psia, $T_0 = 405$ K, and $Re_\infty = 1.75 \times 10^6/\text{ft}$.

Table 2. Assumed values of shock height above wall when $p_{0,i} = 90$ psia and $k = 10.2$ mm. Measuring two diameters off the roughness centerline.

Diameters Downstream	Distance Downstream (mm)	Shock Height (mm)
2.0	11.94	11.93
3.0	17.91	12.83
5.0	29.85	16.73
10.0	59.69	27.33

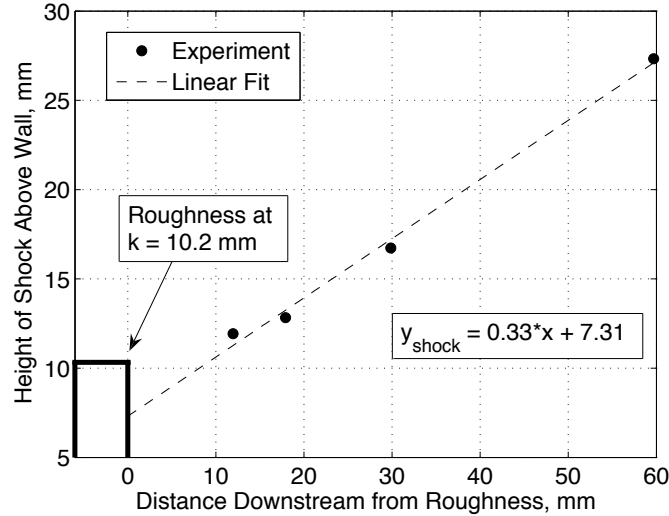


Figure 12. Plot of assumed shock shape behind the roughness in a plane two diameters off-center from the roughness.

IV. Laminar Instability in the Roughness Wake

Under certain conditions, a laminar instability near 21 kHz was observed in the wake of the roughness element. The instability was discovered after results from Danehy et al.¹⁴ (Figure 3) led to a search for instabilities off the roughness centerline. This instability, first reported in Reference 24, is believed to be the first of its kind measured at hypersonic speeds.

The instability was observed two diameters off the centerline of a 10.2-mm roughness during runs with initial tunnel pressures of 75, 80, and 90 psia. The instability was generally observed between stagnation pressures of 70–90 psia, corresponding to stagnation temperatures of 405–433 K and unit Reynolds numbers of $1.7\text{--}2.0 \times 10^6/\text{ft}$. Flow conditions from Harris code²⁹ computations at a stagnation pressure of 80 psia are presented in Table 3. All runs were quiet with a laminar boundary layer on the nozzle wall. The instability was seen for streamwise positions ranging from 1.2–26.8 diameters downstream of the roughness, but no measurements farther downstream were made.

Several tests were performed in order to ensure that the instability is real. A real flow instability:

1. Should be seen on multiple sensor types
2. Should disappear when the roughness is removed
3. Should disappear in freestream when the roughness is present
4. Should have a frequency that varies with Reynolds number
5. Should grow downstream of the roughness

The results of these tests will be summarized in this section (for further details see Reference 25). Stray effects such as vibration and shock/boundary-layer interactions, which could cause an apparent instability to be observed, have yet to be fully ruled out. The largest concern remains an unsteady shock/boundary-layer interaction caused by the roughness, probe, or probe support. Non-intrusive measurements or stability computations are needed for these conditions. Should the computations and experiments agree, the existence of the laminar instability will be confirmed.

A. Instability Seen on Two Sensor Types

The instability was observed during a run when the pitot probe was left stationary at a height of $y = 8.5$ mm with $k = 10.2$ mm. During the entire 2.4-s run, an oscillation near 21 kHz could be seen in the time trace

Table 3. Sample flow conditions where the instability was observed, calculated using the Harris code.²⁹ Stagnation pressure of 80 psia at tunnel axial coordinate $z = 75.9$ in. from throat, near the roughness location.

Boundary-layer height (99.5% of freestream velocity)	δ	9.23 mm
Roughness height	k	10.16 mm
Roughness diameter	D	5.97 mm
Height ratio	k/δ	1.10
Diameter ratio	D/δ	0.65
Tunnel stagnation pressure	p_0	551.58 kPa
Tunnel stagnation temperature	T_0	433 K
Freestream Mach number	M_∞	5.93
Freestream density	ρ_∞	0.024 kg/m ³
Freestream pressure	p_∞	0.37 kPa
Freestream temperature	T_∞	53.9 K
Freestream velocity	u_∞	872.7 m/s
Freestream unit Reynolds number	Re_∞	$6.02 \times 10^6/\text{m}$
Reynolds number at the roughness height k based on conditions in the undisturbed laminar boundary layer at the height k	Re_k	60,800

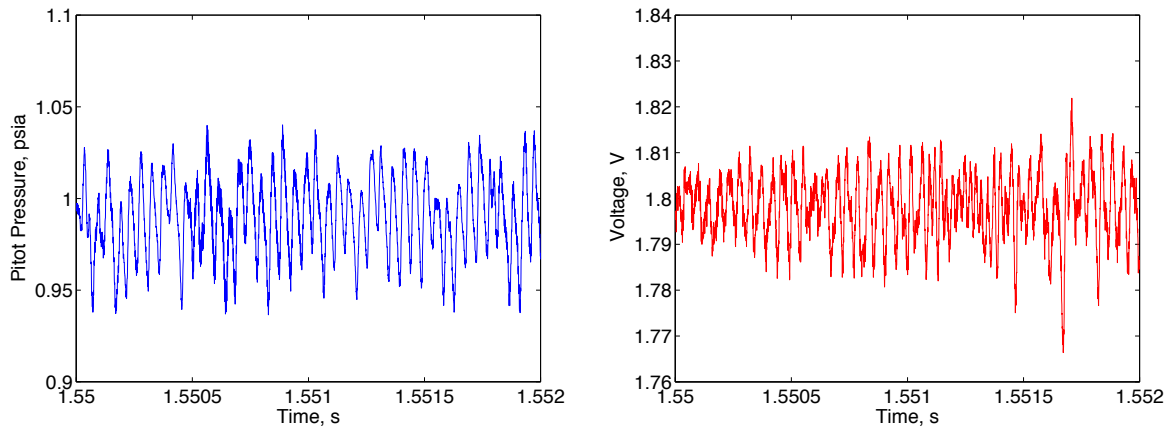
of the pressure signal. The run was repeated at the same conditions using an uncalibrated hot-wire probe instead of the pitot probe. The two signals are shown for comparison in Figures 13(a) and 13(b). The pitot-probe signal was reduced to pressure while the hot-wire signal is reported as uncalibrated voltage. The time traces of both signals show an oscillation near 21 kHz. The uncalibrated voltage from the hot-wire was intended only for qualitative comparison to the pressure waveform.

A spectral analysis was performed on the time traces of the signals from $t = 1.5$ – 1.6 s, as shown in Figure 13(c). The blue spectrum and left axis show the pitot-pressure fluctuation amplitudes, nondimensionalized by the theoretical freestream pitot pressure at Mach 6.0. The red spectrum and right axis show the fluctuations amplitudes from the uncalibrated hot wire. Both spectra show a large peak near 21 kHz, with a narrow frequency band of roughly 3–4 kHz. The amplitude of the peak in the pitot-pressure spectrum indicates a RMS pressure of 0.4% of the freestream pitot pressure. In addition to the 21-kHz peak, a smaller peak near 42 kHz is visible in the pitot-probe spectra. This second peak may be a harmonic of the 21-kHz frequency, but is not visible in the hot-wire spectra. The uncalibrated hot-wire spectra has a peak at 40 kHz from an unknown origin. This particular hot-wire was only tuned to a frequency near 40 kHz due to difficulties with the anemometer. In the future, this experiment should be repeated with a more properly-tuned hot wire.

B. Instability Disappears when the Roughness is Removed

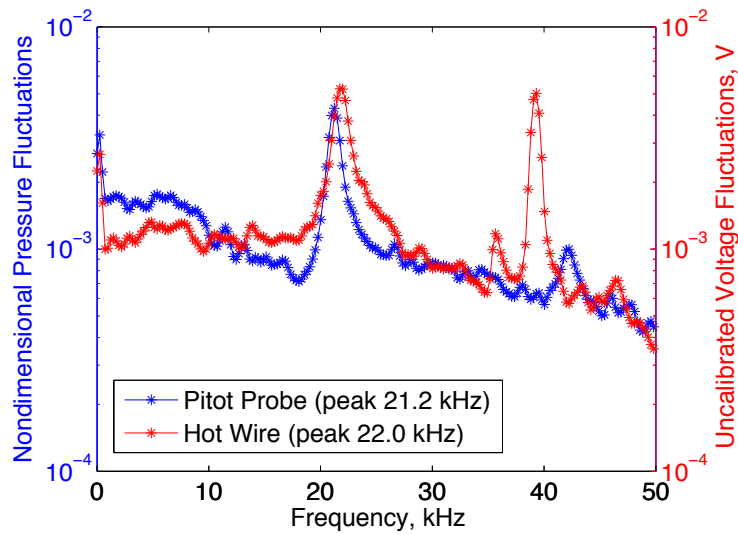
Figure 14 shows a comparison of pitot-pressure spectra from runs with and without the roughness element. The pressure fluctuations were again nondimensionalized by the theoretical freestream pitot pressure at Mach 6.0. The probe was positioned 1.2 diameters downstream of the roughness location and two diameters off the roughness centerline. The data are from a height of 11 mm above the wall, which was the height where the fluctuation levels were near their peak. In the absence of the roughness element, fluctuation levels near 0.01–0.001% (per 0.24 kHz) can be seen, suggesting that the boundary-layer was laminar as expected. A small peak near 13 kHz was seen, which may or may not be a physical instability in the smooth-wall boundary layer. When the roughness height k was 10.2 mm, the fluctuation levels increased by nearly three orders of magnitude. A peak at 21 kHz can be seen with an amplitude of 3% (per 0.24 kHz). Two harmonics are visible at 42 kHz and 63 kHz.

Table 4 shows the RMS pitot-pressure fluctuations from Figure 14, calculated by integrating the area under the power spectrum and nondimensionalized by the freestream pitot pressure. The RMS of the signal



(a) Kulite

(b) Hot Wire



(c) RMS spectra from $t=1.5-1.6$ s

Figure 13. Time trace and spectra of 21-kHz disturbance using two different sensors at similar conditions. Measuring two diameters off-center from roughness and 1.2 diameters downstream. $p_{0,i} = 90$ psia, $k = 10.2$ mm, and $y = 8.5$ mm. Pitot-pressure fluctuations from spectrum are nondimensionalized by freestream pitot pressure. Uncalibrated voltage fluctuations from the hot wire are shown.

from 0–100 kHz increases from 0.05% to 5.1% when the roughness is present. The instability peak (19–23 kHz) has an RMS of 4.1% when the roughness is present.

C. Instability Disappears in Freestream when the Roughness is Present

An instability within the wake of the roughness element would be expected to disappear away from the wall in the freestream flow. At an initial stagnation pressure of 90 psia, the RMS of the 21-kHz instability was examined at 1.2 diameters downstream and two diameters off-center from the roughness. Three runs were performed with the pitot probe moving in the wall-normal direction. Each run began at a different initial height above the wall y_i and the probe was moved either towards or away from the wall. Using the power spectrum, the area under the 21-kHz peak was integrated from 19–23 kHz to find the RMS of the frequency band. The RMS was nondimensionalized by the freestream pitot pressure.

Figure 15 shows the root-mean-square pressure fluctuations of the 19–23 kHz frequency band at various heights above the wall. A red horizontal line denotes the roughness height of 10.2 mm. The 21-kHz instability increases away from the wall, peaking at a height near the roughness height. The peak fluctuations are around 2.5% of the freestream pitot pressure. At heights greater than 15 mm, the RMS decreases to near zero in the freestream. This pattern suggests an instability is being detected.

D. Frequency of Instability Varies with Reynolds Number

A test was performed to examine how the frequency of the instability depends on freestream Reynolds number. During a single run, the pitot probe was left stationary 1.2 diameters downstream and two diameters off-center from the roughness. The probe was at a height of 10.6 mm above the wall and the roughness height was 10.2 mm. In the BAM6QT, the decreasing stagnation pressure during the run causes the freestream Reynolds number to decrease. Figure 16 shows four spectra from a run with an initial stagnation pressure of 90 psia. Spectra from the pressure signal were computed at several 0.05-s intervals during the run at different Reynolds numbers. During the run, the instability peak frequency decreases from 22.5 kHz to 20.75 kHz. The instability frequency decreases by 8% as the Reynolds number decreases by 5%. The variation of frequency with Reynolds number suggests that the instability is real.

E. Instability Grows Downstream of the Roughness

A final test was performed to observe growth of the instability downstream of the roughness.²⁴ Measurements in the wake of the $k = 10.2$ -mm roughness were performed using a calibrated hot wire at a constant Reynolds number. A hot-wire probe was used because the Kulite pitot probe tended to resonate with large amplitude when measuring far downstream from the roughness. In addition, the hot wire interferes less with the flow.

The hot wire was moved to several streamwise locations at a constant height above the wall of $y = 10.2$ mm, near the instability peak amplitude in Figure 15. Several runs were performed at an initial stagnation pressure of 80 psia. Root-mean-square spectra were calculated from a similar time during the run ($t = 1.00$ – 1.05 s) so that the freestream conditions would be similar. The mass-flux fluctuations (per 0.24 kHz) were nondimensionalized by the mean mass flux.

Figure 17 shows the results, with a typical pre-run background noise spectrum shown for comparison. Each spectrum downstream of the roughness shows a peak at 21 kHz. At 1.6 roughness diameters downstream, the RMS of the 21-kHz peak was 1% of the mean mass flux and the background levels were 0.1–0.5%. At 13 diameters downstream the RMS of the 21-kHz peak grew to 3% and the background noise levels grew higher. A peak at 65 kHz was observed at both 1.6 and 13 diameters downstream and could be a second instability. At 26.8 diameters downstream the 21-kHz peak had a RMS of 20% of the mean with higher background levels. When the probe was placed 7.6 diameters upstream of the roughness element, the spectra was similar to the pre-run values, as expected for a laminar boundary layer. There was no evidence of the 21-kHz disturbance upstream of the roughness element, suggesting that the disturbance is not likely to be vibration of the probe support.

Table 5 shows the RMS mass-flux fluctuations from the data in Figure 17, calculated by integrating the area under the power spectrum and nondimensionalized by the mean mass flux. When calculating the RMS using this method, the 21-kHz peak has an amplitude of 35.0% of the mean at 26.8 diameters downstream, while the total signal RMS is 43.0%.

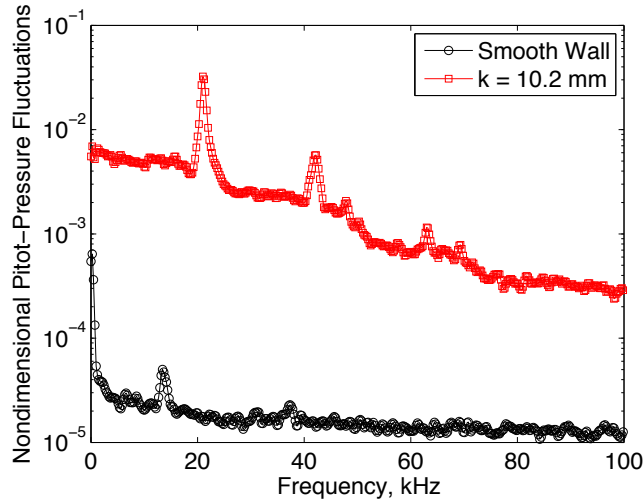


Figure 14. Comparison of spectra with and without the roughness at $p_{0,i} = 90$ psia. Spectra at a height of 11 mm above the wall, 1.2 diameters downstream from the roughness element and two diameters off the centerline. Pitot-pressure fluctuations nondimensionalized by freestream pitot pressure.

Table 4. RMS pitot-pressure fluctuations from Figure 14, nondimensionalized by the freestream pitot pressure. The RMS was calculated by integrating the area under the power spectrum.

	Smooth Wall	$k = 10.2$ mm
Total (0–100 kHz)	0.05%	5.1%
Peak (19–23 kHz)	–	4.1%

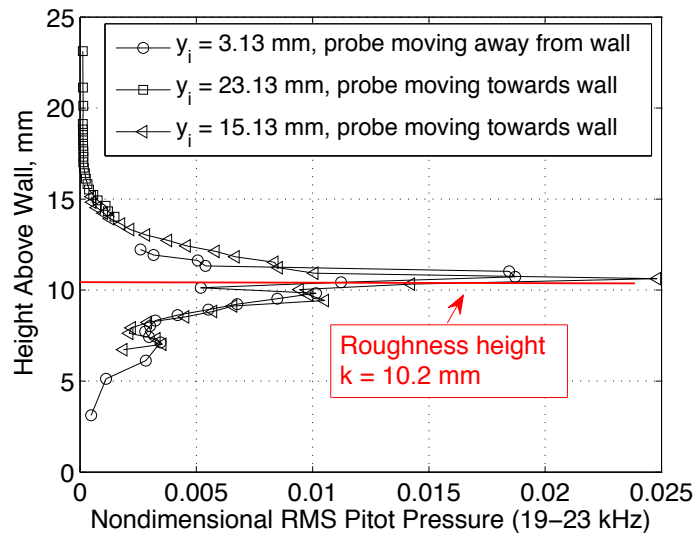


Figure 15. RMS pressure fluctuations in the 19–23 kHz frequency band, nondimensionalized by the theoretical freestream pitot pressure. Three runs with probe at 1.2 diameters downstream of the roughness and two diameters off the centerline, traversing in one of two directions during the run. Peak in RMS seen near roughness height of 10.2 mm.

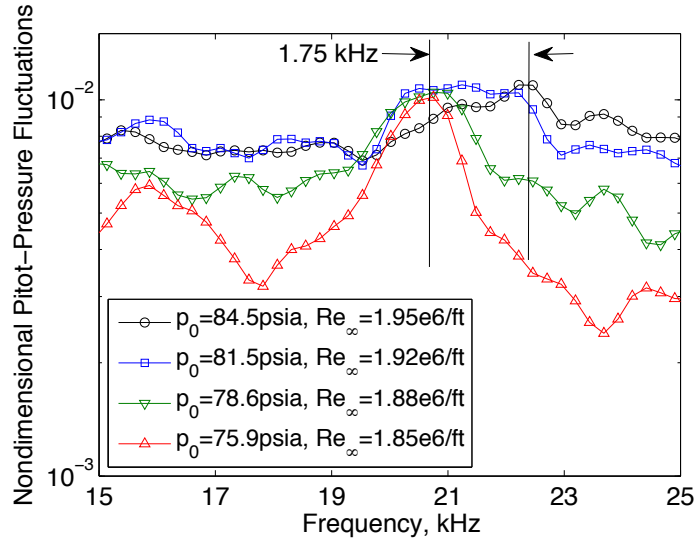


Figure 16. Frequency shifting of instability with Reynolds number. Measuring 1.2 diameters downstream, two diameters off-center from the roughness, and 10.6 mm above the wall. Pitot-pressure fluctuations nondimensionalized by freestream pitot pressure.

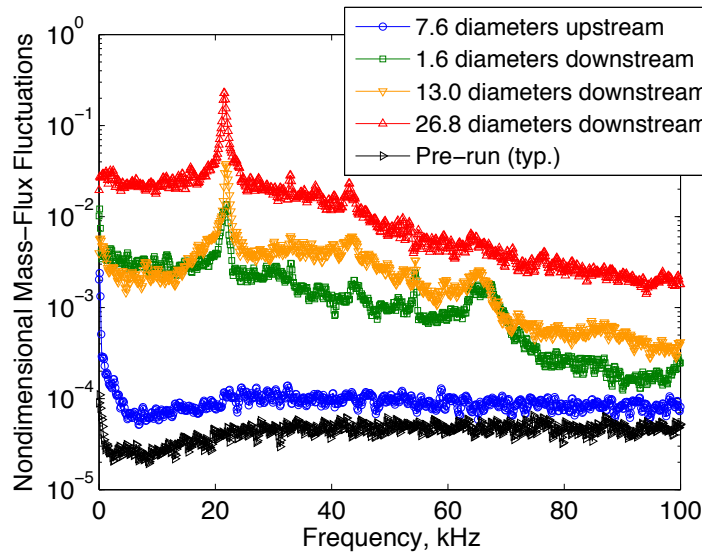


Figure 17. RMS spectra at a height of $y = 10.2$ mm above the wall, measuring two diameters off-center from the $k = 10.2$ mm roughness. Mass-flux fluctuations nondimensionalized by mean mass flux. All runs were at an initial stagnation pressure of 80 psia and the spectra are from $t = 1$ s during the run ($p_0 = 75$ psia and $Re_\infty = 1.75 \times 10^6$ /ft).

Table 5. RMS mass-flux fluctuations from Figure 17, nondimensionalized by the mean mass flux. The RMS was calculated by integrating the area under the power spectrum.

	7.6D upstream	1.6D downstream	13D	26.8D
Total (0–100 kHz)	0.2%	4.1%	7.3%	43.0%
Peak (19–23 kHz)	–	2.5%	5.4%	35.0%

F. Summary of Laminar Instability

The evidence suggests that a laminar instability has been measured in the wake of the roughness. The instability was observed using two different sensor types at similar conditions. Tests have shown that the instability is strongest off the centerline at a height near the roughness height, and disappears in the freestream. In addition, the frequency of the instability varies with Reynolds number. The instability was seen to grow to large amplitudes downstream of the roughness, with RMS values approaching 35% of the mean mass flux. Though stray effects such as shock/boundary-layer interactions have yet to be fully ruled out, this appears to be the first time that an instability has been detected in a roughness wake at hypersonic speeds.

Mean-flow and instability computations are being carried out for comparison to these experiments at UCLA³² and NASA Langley.³³ If good agreement is obtained, both computation and experiment will be validated. The longer-term goal is to develop e^N -class methods for predicting transition in flight and in large wind tunnels, where measurements of the roughness wake and its instabilities do not appear feasible.

V. Conclusion

A roughness element was installed on the nozzle wall of the Boeing/AFOSR Mach-6 Quiet Tunnel in order to make quantitative measurements of instabilities within the wake. These measurements will be used to support the development of computational methods for predicting roughness-induced transition.

Using the pitot probe and hot-wire probes, measurements of the mean flow and fluctuations within the wake of the roughness were performed while searching for instabilities. Mean-flow pitot-pressure profiles were collected for various roughness heights and can be used to compare to future computations. At a roughness height of 10.2 mm and tunnel stagnation pressures of 70–90 psia, a flow instability near 21 kHz was discovered within the laminar boundary layer. The instability was observed using two different sensors and the frequency was observed to vary with Reynolds number. When the roughness is removed or the probe is placed upstream of the roughness, the instability disappears. The instability is strongest off the centerline at a height near the roughness height, where a shear layer should be present, and was observed to grow downstream. Though stray effects such as vibration or shock/boundary-layer interactions have yet to be fully ruled out, the measurement of a roughness-induced instability appears to be the first at hypersonic speeds. Computations are in progress, and if agreement can be obtained the results will be validated.

Future work will include a study of the roughness-induced instability in greater detail. Measurements will be made in support of computations in order to develop a physics-based method for predicting hypersonic transition induced by an isolated roughness element.

Acknowledgments

This research was funded by NASA under grant 102361.

References

- ¹Steven P. Schneider. Flight Data for Boundary-Layer Transition at Hypersonic and Supersonic Speeds. *Journal of Spacecraft and Rockets*, 36(1):8–20, January-February 1999.
- ²Kenneth F. Stetson. On Predicting Hypersonic Boundary Layer Transition. Technical Report AFWAL-TM-87-160-FIMG, Flight Dynamics Laboratory, Air Force Wright Aeronautical Laboratories, Wright-Patterson Air Force Base, Ohio, March 1987.
- ³Eli Reshotko. Transition Issues for Atmospheric Entry. *Journal of Spacecraft and Rockets*, 45(2):161–164, March-April 2008.
- ⁴Steven P. Schneider. Effects of Roughness on Hypersonic Boundary-Layer Transition. *Journal of Spacecraft and Rockets*, 45(2):193–209, March-April 2008.
- ⁵Scott A. Berry, Aaron H. Auslender, Arthur D. Dilley, and John F. Calleja. Hypersonic Boundary-Layer Trip Development for Hyper-X. *Journal of Spacecraft and Rockets*, 38(6):853–864, November-December 2001.
- ⁶Matthew P. Borg and Steven P. Schneider. Effect of Freestream Noise on Roughness-Induced Transition for the X-51A Forebody. *Journal of Spacecraft and Rockets*, 45(6):1106–1116, November-December 2008.
- ⁷Katya M. Casper, Brad M. Wheaton, Heath B. Johnson, and Steven P. Schneider. Effect of Freestream Noise on Roughness-Induced Transition at Mach 6. AIAA Paper 2008-4291, June 2008.
- ⁸B. Anderson and Charles H. Campbell et al. BLT Flight Experiment Overview and In-Situ Measurements. AIAA Paper 2010-0240, to appear at 48th AIAA Aerospace Science Meeting, January 2010.
- ⁹Thomas J. Horvath, D. Tomek, S. Splinter, J. Zalameda, P. Krasa, R. Schwartz, D. Gibson, and A. Tietjen. The Hythirm

Project: Flight Thermography of the Space Shuttle During Hypersonic Re-Entry. AIAA Paper 2010-0241, to appear at 48th AIAA Aerospace Sciences Meeting, January 2010.

¹⁰National Aeronautics and Space Administration. *Photo ISS011-E-11074, Cropped*, July 2005 (accessed August 13, 2009). <http://spaceflight.nasa.gov/gallery/images/station/crew-11/html/iss011e11074.html>.

¹¹National Aeronautics and Space Administration. *Photo S114-E-6215, Cropped*, July 2005 (Accessed September 14, 2009). <http://spaceflight.nasa.gov/gallery/images/shuttle/sts-114/html/s114e6215.html>.

¹²Daniel C. Reda. Review and Synthesis of Roughness-Dominated Transition Review and Synthesis of Roughness-Dominated Transition Correlations for Reentry Applications. *Journal of Spacecraft and Rockets*, 39(2):161–167, March–April 2002.

¹³Allen H. Whitehead. Flow Field and Drag Characteristics of Several Boundary-Layer Tripping Elements in Hypersonic Flow. Technical Report TN D-5454, NASA Langley Research Center, October 1969.

¹⁴Paul M. Danehy, Brett Bathel, Christopher Ivey, Jennifer A. Inman, and Stephen B. Jones. NO PLIF Study of Hypersonic Transition over a Discrete Hemispherical Roughness Element. AIAA Paper 2009-394, January 2009.

¹⁵M. S. Acarlar and C. R. Smith. A Study of Hairpin Vortices in a Laminar Boundary Layer. Part 1. Hairpin Vortices Generated by a Hemisphere Protuberance. *Journal of Fluid Mechanics*, 175:1–41, 1987.

¹⁶Chau-Lyan Chang and Meelan M. Choudhari. Hypersonic Viscous Flow over Large Roughness Elements. AIAA Paper 2009-0173, January 2009.

¹⁷Meelan Choudhari, Fei Li, and Jack Edwards. Stability Analysis of Roughness Array Wake in a High-Speed Boundary Layer. AIAA Paper 2009-0170, January 2009.

¹⁸F. Gokhan Ergin and Edward B. White. Unsteady and Transitional Flows Behind Roughness Elements. *AIAA Journal*, 44(11):2504–2514, November 2006.

¹⁹Eli Reshotko and Anatoli Tumin. Role of Transient Growth in Roughness-Induced Transition. *AIAA Journal*, 42(4):766–770, April 2004.

²⁰R. W. Wlezien. Measurements of Acoustic Receptivity. AIAA Paper 94-2221, June 1994.

²¹P. S. Klebanoff and K. D. Tidstrom. Mechanism by Which a Two-Dimensional Roughness Element Induces Boundary-Layer Transition. *The Physics of Fluids*, 15(7):1173–1188, July 1972.

²²Steven P. Schneider. Development of Hypersonic Quiet Tunnels. *Journal of Spacecraft and Rockets*, 45(4):641–664, July–August 2008.

²³Thomas J. Juliano, Steven P. Schneider, Selin Aradag, and Doyle Knight. Quiet-Flow Ludwig Tube for Hypersonic Transition Research. *AIAA Journal*, 46(7):1757–1763, July 2008.

²⁴Brad M. Wheaton, Thomas J. Juliano, Dennis C. Berridge, Amanda Chou, Peter L. Gilbert, Katya M. Casper, Laura E. Steen, Steven P. Schneider, and Heath B. Johnson. Instability and Transition Measurements in the Mach-6 Quiet Tunnel. AIAA Paper 2009-3559, June 2009.

²⁵Bradley M. Wheaton. Roughness-Induced Instability in a Laminar Boundary Layer at Mach 6. Master’s thesis, Purdue University School of Aeronautics & Astronautics, West Lafayette, IN, December 2009.

²⁶Thomas J. Juliano, Rodrigo Segura, Matthew P. Borg, Katya Casper, Michael J. Hannon, Jr., Brad M. Wheaton, and Steven P. Schneider. Starting Issues and Forward-Facing Cavity Resonance in a Hypersonic Quiet Tunnel. AIAA Paper 2008-3735, June 2008.

²⁷Shann J. Rufer and Steven P. Schneider. Hot-Wire Measurements of Instability Waves on a Blunt Cone at Mach-6. AIAA Paper 2005-5137, June 2005.

²⁸Shann J. Rufer. *Hot-Wire Measurements of Instability Waves on Sharp and Blunt Cones at Mach 6*. PhD thesis, Purdue University School of Aeronautics & Astronautics, West Lafayette, IN, December 2005.

²⁹Steven P. Schneider. Design of a Mach-6 Quiet-flow Wind Tunnel Nozzle using the e**N Method for Transition Estimation. AIAA Paper 1998-0547, January 1998.

³⁰M. V. Morkovin and W. S. Bradfield. Probe Interference in Measurements in Supersonic Laminar Boundary Layers. *Journal of the Aeronautical Sciences*, 21:785–787, November 1954.

³¹James M. Kendall, Jr. An Experimental Investigation of Leading-Edge Shock-Wave-Boundary-Layer Interaction at Mach 5.8. *Journal of the Aeronautical Sciences*, 24:47–56, January 1957.

³²Patrick T. Greene, Jeff D. Eldredge, Xiaolin Zhong, and John Kim. A Numerical Study of Purdue’s Mach 6 Tunnel with a Roughness Element. AIAA Paper 2009-174, January 2009.

³³Chau-Lyan Chang, Meelan M. Choudhari, and Fei Li. Numerical Computations of Hypersonic Boundary-Layer over Surface Irregularities. AIAA Paper 2010-1572, to appear at 48th AIAA Aerospace Science Meeting, January 2010.